3rd European supercritical CO_2 Conference
September 19-20, 2019, Paris, France

2019-sCO2.eu-108

TURBULENCE MODELLING FOR SUPERCRITICAL CO_2 FLOWS IN A VERTICAL TUBE

Gustavo J. Otero R.*
Process and Energy Department Mechanical Engineering Delft University of Technology
Delft, the Netherlands
Email: g.j.oterorodriguez@tudelft.nl

Luis F. González-Portillo
Grupo de Investigaciones Termoenergeticas (GIT)
Universidad Politécnica de Madrid
Madrid, Spain
Email: lf.gonzalez@upm.es

Rene Pecnik
Process and Energy Department
Mechanical Engineering Delft
University of Technology
Delft, the Netherlands
Email: r.pecnik@tudelft.nl

ABSTRACT

Standard eddy viscosity models are incapable of accounting for the effects of strong variation of thermophysical properties on turbulence of supercritical fluids [1], which can cause considerable inaccuracies in the prediction of the pressure drop, the heat transfer coefficient, and other quantities of interest for supercritical flows. In our previous research [2], we have developed consistent modifications for eddy viscosity models to make them more reliable for wall-bounded turbulent flow with sharp gradients in the thermophysical properties. In this paper, we implement these density-corrected turbulence models to our in-house Reynolds-Averaged Navier-Stokes (RANS) solver to simulate an upward heated turbulent pipe flow with CO_2 at supercritical pressure. The results show an improvement in the accuracy of the model for the force convection test cases. However, when heat transfer deterioration is present, the modified turbulence model is still not reliable. To investigate the cause of the inaccuracy, we introduced different methods to model the turbulent heat flux, by changing the constant value of the turbulent Prandtl number and using two different algebraic equations. As expected, the model for the turbulent Prandtl number considerably influences the overall simulation prediction. To better model heat transfer deterioration in an upward flow of a turbulent supercritical flow, a better approximation of the turbulent heat flux is necessary.

1. INTRODUCTION

Supercritical fluids — fluids above the critical pressure — have recently been considered for many engineering applications, in particular in the field of energy generation [3]. For instance, thermodynamics power cycles can use supercritical fluids as the working fluid [4-5]. Moreover, renewable energy technologies, like solar energy and waste heat recovery, can benefit from the advantage of supercritical fluids [4, 6]. Other industrial processes with supercritical fluids include pharmaceutical processes or enhanced oil recovery [7]. All these applications require a comprehensive understanding of fluid dynamics and heat transfer of supercritical fluids to correctly design and model the system.

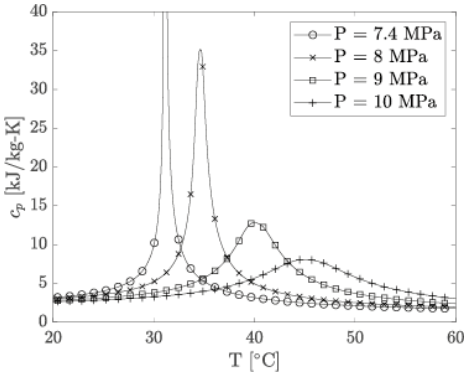

Figure 1. Variation of specific heat capacity as a function of temperature for constant pressure for CO_2

Supercritical fluids exhibit deviations from ideal thermodynamic behavior and do not have a recognizable phase change; the fluid transition from a liquid-like and gas-like phase occurs in a continuous manner. However, small changes in temperature and/or pressure in the supercritical region can lead to strong gradients on the thermophysical properties. For example, figure 1 shows the variation of the specific heat

* corresponding author(s)

DOI: 10.17185/duepublico/48872

capacity at constant pressure, c_p, as a function of temperature for CO_2 ($p_{cr} = 7.39$ MPa). The pseudo-critical temperature is the location where c_p has its peak at constant pressure. These abrupt variations of thermophysical properties of a supercritical fluid results in a flow behavior and a heat transfer which is different from an ideal gas flow [8].

In a heated upward flowing supercritical fluid, heat transfer deterioration may occur [9]. The sharp variation of thermophysical properties in the critical region and the effect of buoyancy influence turbulence, which could result in heat transfer deterioration [10].

Direct numerical simulations (DNS) have been performed to analyze the heat transfer to supercritical fluids in turbulent pipe flows [9,10]. But, these highly accurate simulations are limited to simple geometries and low Reynolds numbers due to the high computational cost needed. To bypass the computational cost, it is possible to solve the RANS equations coupled with eddy viscosity models. However, these models rely on a limited data, and their development is hampered by the lack of knowledge on supercritical fluids and heat transfer deterioration.

There are three challenges for modeling turbulence of an upward flowing supercritical fluid.

1. **Eddy viscosity:** an eddy viscosity model must properly account for variations in the thermophysical properties. Most models have been developed for incompressible flows and the effect of density on turbulence is not accounted for. We have proposed in our recent study [2] how eddy viscosity models can be modified to successfully account for this effect. The proposed modifications are generally applicable to any turbulence model and are based on analytic scaling arguments.
2. **Turbulent heat flux:** the model for the turbulent heat flux must account for variations in molecular Prandtl number across the boundary layer. Commonly, the turbulent heat flux is modelled using the analogy between turbulent momentum and heat flux by means of a turbulent Prandtl number (Pr_t). Several models have been developed and applied to ideal gas flows [11, 12]. It is known that in case of heat transfer deterioration, the definition of the turbulent Prandtl number is not applicable. The heat deterioration causes an inflection point in the streamwise velocity profile making $Pr_t \to \infty$ [10].
3. **Buoyancy production of turbulent kinetic energy:** the eddy viscosity model must account for the buoyancy production of turbulent kinetic energy (TKE). Also here, most of the models for the buoyancy production in the TKE equation assume the ideal gas law to relate density with temperature fluctuations [13]. Additional insight from DNS is required to develop accurate models to account for buoyancy effects.

This article investigates the accuracy of RANS turbulence model to predict heat transfer in a turbulent pipe flow with CO_2 at supercritical pressure. Three standard turbulence models, namely the Myong-Kasagi (MK) [14], Menter's $k-\omega$ SST [15], and Spallart-Allmaras (SA) [16] turbulence models are used to model the Reynolds stresses. The density modifications derived in our previous study [2] are included into the turbulence models to solve the system. Moreover, we investigate the influence of the turbulent Prandtl number on the heat transfer. Finally, two different algebraic models for the turbulent Prandtl number [11,12] are used to approximate the turbulent heat flux.

2. TEST CASE

2.1 Experimental data

In literature, experimental data is available to investigate turbulent heat transfer to supercritical fluids. For the present article, two data sources [17,18] are chosen to study the heat transfer deterioration of flows near the supercritical point. These studies experimented with CO_2 flowing upwards in a uniformly heated pipe at different conditions. The boundary conditions of these experiments are summarized in table 1. We will use the measured wall temperature to compare the simulations with the experiments; figure 2 shows the measured wall temperature from the selected experimental data.

The experiments of case 1, taken from Bae et al. [17], are shown in figure 2a. The case with the lowest heat flux ($q" = 29.3\ \mathrm{kW/m^2}$) is not affected by heat transfer deterioration; this can be seen by the smooth increase of wall temperature. For the experiment with the highest heat flux ($q" = 48.8\ \mathrm{kW/m^2}$), the larger wall temperature at the beginning of the measurements indicate heat transfer deterioration. Heat transfer deterioration decreases when the bulk temperature is close to the pseudo-critical value. For these experiments, the measurements are collected half a meter after the wall heating starts, thus no data is available at the inflow.

The experiments for case 2, reported by Kim et al. [18], show a more detailed quantification of the heat transfer deterioration. Figure 2b shows the wall temperature along the pipe. Heat transfer deterioration can be seen for a heat flux of $23\ \mathrm{kW/m^2}$ and $30\ \mathrm{kW/m^2}$ when the wall temperature crosses the pseudo-critical temperature. The wall temperature shows one or two steep peaks, characteristic of heat transfer deterioration.

2.2 Governing equations

In the present study, the RANS equations, written in cylindrical coordinates, are solved. To close the system of equations, an equation of state (EOS) is used to define the relation between density, pressure, temperature and internal energy. The multi-parameter equation of state of Kunz and Wagner [19] is used for CO_2.

DOI: 10.17185/duepublico/48872

Table 1. Experimental cases investigated, where p^* is the pressure, T_o^* is the inlet temperature, D^* is the pipe diameter, G^* is the mass flux and the accent "*" refers to a dimensional quantity. Re_0 and Pr_0 are the Reynolds and Prandtl number, respectively, at the inflow.

	p^* [MPa]	T_0^*[°C]	D^* [mm]	G^* [kg/(s m^2)]	q" [kW/m^2]	Re_0 [-]	Pr_0 [-]
Case 1 [17]	8.12	5	6.32	400	29.3	2,500	2.14
	8.12	5	6.32	400	48.8	2,500	2.14
Case 2 [18]	8	15	7.8	314	20.0	29,000	2.3
	8	15	7.8	314	23.0	29,000	2.3
	8	15	7.8	314	30.0	29,000	2.3

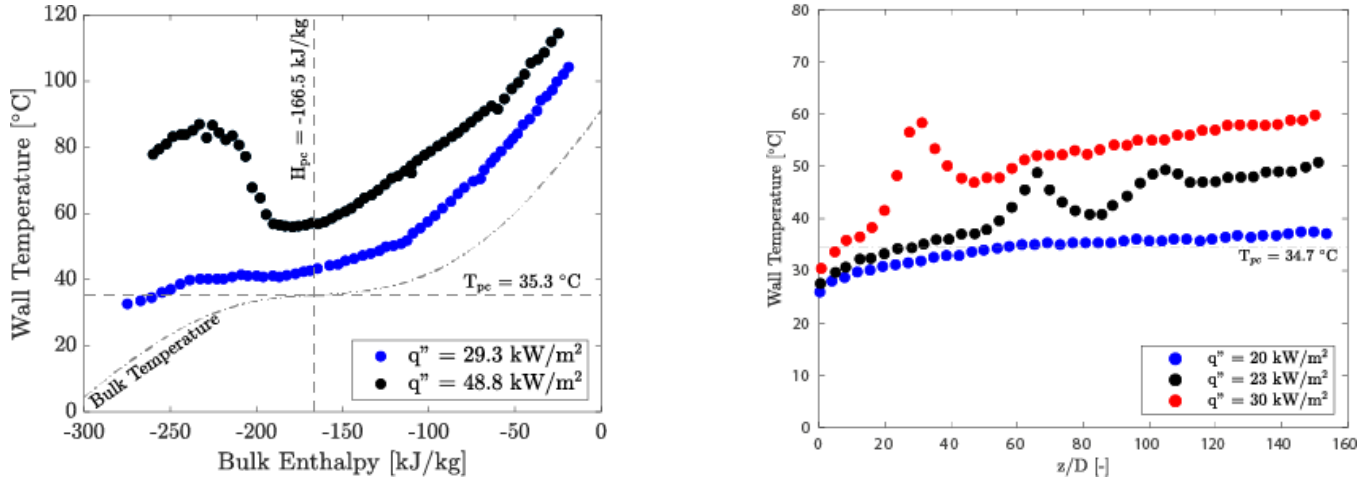

Figure 2. Wall temperature distribution as a function of the pipe stream-wise distance for two experimental set-up: (a) Bae et al [17] and (b) Kim et al. [18]. The bulk enthalpy can be seen as the pipe distance because a constant heat flux is introduced into the system. These figures were directly reproduced from the references [17,18]

The governing equations for momentum, in radial and stream-wise direction, and the energy can be expressed in their non-dimensional form (scaled by wall units), and assuming a two-dimensional steady-state axis-symmetric flow as:

- for momentum in stream-wise direction,

$$\frac{\partial\langle\rho\rangle\{u_z\}^2}{\partial z}+\frac{1}{r}\frac{\partial\, r\langle\rho\rangle\{u_z\}\{u_r\}}{\partial r}=-\frac{\partial\langle p\rangle}{\partial z}+\frac{\langle\rho\rangle}{Fr_0^2}+\frac{\partial}{\partial z}\left[\left(\frac{\langle\mu\rangle}{Re_\tau}+\mu_t\right)\left(2\frac{\partial\{u_z\}}{\partial z}-\frac{2}{3}\nabla.\{\boldsymbol{u}\}\right)\right]+\frac{1}{r}\frac{\partial}{\partial r}\left[r\left(\frac{\langle\mu\rangle}{Re_\tau}+\mu_t\right)\left(\frac{\partial\{u_z\}}{\partial r}+\frac{\partial\{u_r\}}{\partial z}\right)\right],$$

- for momentum in radial direction,

$$\frac{1}{r}\left[\frac{\partial r\langle\rho\rangle\{u_z\}\{u_r\}}{\partial z}+\frac{\partial\, r\langle\rho\rangle\{u_r\}^2}{\partial r}\right]=-\frac{\partial\langle p\rangle}{\partial r}+\frac{1}{r}\frac{\partial}{\partial r}\left[r\left(\frac{\langle\mu\rangle}{Re_\tau}+\mu_t\right)\left(2\frac{\partial\{u_r\}}{\partial r}-\frac{2}{3}\nabla.\{\boldsymbol{u}\}\right)\right]+\frac{\partial}{\partial z}\left[\left(\frac{\langle\mu\rangle}{Re_\tau}+\mu_t\right)\left(\frac{\partial\{u_z\}}{\partial r}+\frac{\partial\{u_r\}}{\partial z}\right)\right]-\frac{1}{r}\left(\frac{\langle\mu\rangle}{Re_\tau}+\mu_t\right)\left(2\frac{\{u_r\}}{r}-\frac{2}{3}\nabla.\{\boldsymbol{u}\}\right),$$

- and energy,

$$\frac{\partial\langle\rho\rangle\{H\}\{u_z\}}{\partial z}+\frac{1}{r}\frac{\partial\, r\langle\rho\rangle\{H\}\{u_r\}}{\partial r}=\frac{1}{r}\frac{\partial}{\partial r}\left[r\left(\frac{\langle\lambda\rangle/Cp}{Re_\tau Pr}+\frac{\mu_t}{Pr_t}\right)\frac{\partial\{H\}}{\partial r}\right]+\frac{\partial}{\partial z}\left[\left(\frac{\langle\lambda\rangle/Cp}{Re_\tau Pr}+\frac{\mu_t}{Pr_t}\right)\frac{\partial\{H\}}{\partial z}\right],$$

where H is the specific enthalpy, u_z and u_r are the streamwise (axial) and radial velocity component, respectively. $\nabla.\{\boldsymbol{u}\}$ is the divergence of the velocity vector in cylindrical coordinates. The dimensionless parameters $Re_\tau=u_\tau\rho_w^*D^*/\mu_w^*$ and $Fr_0=u_\tau/\sqrt{g^*D^*}$ are the friction Reynolds number and the Froude number, where $u_\tau=\sqrt{\tau_w/\rho_w^*}$ is the friction velocity. The Froude number takes into account the buoyancy effects with g^* the gravitational acceleration. In the RANS equations, we use the Reynolds decomposition for most of the quantities, defined as: $\phi=\langle\phi\rangle+\phi'$ with $\langle\phi'\rangle=0$, and the Favre decomposition for the velocity and enthalpy, defined as: $\phi=\{\phi\}+\phi"$ with $\langle\rho\rangle\{\phi\}=\langle\rho\phi\rangle$, $\langle\rho\rangle\{\phi"\}=0$, and $\langle\phi"\rangle\neq0$.

3. TURBULENCE MODELLING

The Reynolds shear stress and turbulent heat flux are modelled in the above equations by the Boussinesq

DOI: 10.17185/duepublico/48872

approximation $\left(\langle\rho u"_i u"_j\rangle = 2\mu_t\{S_{ij}\} - 2/3\langle\rho\rangle k\delta_{ij}\right)$ and the gradient diffusion hypothesis $(\langle\rho u"_i H"\rangle = \mu_t/Pr_t\ \partial\{H\}/\partial x_i)$, respectively, adding two extra unknowns to the system of equations: the eddy viscosity (μ_t) and the turbulent Prandtl number (Pr_t). In this section, we will discuss how these unknowns are modelled. Moreover, at the end of this section, we briefly discuss the model used for the buoyancy production of turbulence (G_k).

3.1 Turbulence modeling for heated flows with buoyancy

We apply standard (SA, SST, and MK) and variable density turbulence models. We use our recently derived variable density modifications to alter standard turbulence models [2]. In this section, we report how the density modifications for turbulence models are derived.

The semi-local scaling (SLS), as proposed by Huang *et al.* in 1995 [20], is based on the wall shear stress τ_w and on the local mean (instead of wall) values of the density and the viscosity to account for changes in viscous scales due to mean variations in the thermophysical properties. The aim of the SLS was to collapse turbulence statistics for compressible flows at high Mach numbers with those of incompressible flows. In the SLS framework, the friction velocity and viscous length scale are defined as $u_\tau^\star = \sqrt{\tau_w/\langle\rho^*\rangle}$ and $\delta_v^\star = \langle\mu^*\rangle/\langle\rho^*\rangle u_\tau^\star$ respectively. Accordingly, the semi-local wall distance can be defined as $y^\star = y^*/\delta_v^\star$ and the semi-local Reynolds number as,

$$Re_\tau^\star = \frac{u_\tau^\star\,\langle\rho^*\rangle\,D^*}{\langle\mu^*\rangle} = \sqrt{\frac{\langle\rho^*\rangle}{\rho_w^*}}\frac{\mu_w^*}{\langle\mu^*\rangle}Re_\tau,$$

where Re_τ and u_τ (both defined above), are the conventional friction Reynolds number and friction velocity based on viscous wall units. In general, any flow variable can be non-dimensionalized using wall-based units and semi-local units.

Instead of exclusively using the semi-local scaling to collapse turbulence statistics for compressible flows with different Mach numbers, Pecnik and Patel [21] extended the use of the scaling to derive an alternative form of the TKE equation for wall-bounded flows with a strong wall-normal variations of density and viscosity. Starting from the semi-locally scaled non-conservative form of the momentum equations, and with the assumption that the wall shear stress τ_w changes slowly in the stream-wise direction, the SLS TKE equation reads,

$$t_\tau^\star\frac{\partial\hat{\rho}\hat{k}}{\partial t^*} + \frac{\partial\hat{\rho}\hat{k}\hat{u}_j}{\partial\hat{x}_j} = \hat{P}_k + \hat{G}_k - \hat{\rho}\hat{\varepsilon} + \frac{\partial}{\partial\hat{x}_j}\left[\left(\frac{\hat{\mu}}{Re_\tau} + \frac{\hat{\mu}_t}{\sigma_k}\right)\frac{\partial\hat{k}}{\partial\hat{x}_j}\right],$$

with $\hat{P}_k$ as the turbulent production, $\hat{G}_k$ as the buoyancy production, and $t_\tau^\star = D^*/u_\tau^\star$. For brevity with express the TKE equation with Cartesian notation; the derivation is equivalent in cylindrical coordinates. In the equation above, the semi-locally scaled quantities are denoted with the accent "^", as $\hat{\phi}$. If this form of the TKE equation is used in conjunction with a turbulence model — MK and SST — the results for turbulent flows with large thermophysical property variations significantly improve [21]. However, for general industrial applications with complex geometries, it is not feasible to solve the semi-locally scaled equations. The reason is that all turbulence variables would need to be rescaled every iteration step by quantities that depend on the wall friction at the closest wall and by local quantities of density and viscosity.

To overcome the dependence on the wall friction and local quantities, we convert the previous equation back to conventional scales, in particular to viscous wall units. The transformation from SLS quantities to locally-scaled, was performed to each term and after algebraic manipulation we end up with,

$$t_\tau\frac{\partial\langle\rho\rangle k}{\partial t} + \frac{\partial\langle\rho\rangle k\,\{u_j\}}{\partial x_j} =$$
$$P_k + G_k - \langle\rho\rangle\varepsilon + \frac{1}{\sqrt{\langle\rho\rangle}}\frac{\partial}{\partial x_j}\left[\frac{1}{\sqrt{\langle\rho\rangle}}\left(\frac{\langle\mu\rangle}{Re_\tau} + \frac{\mu_t}{\sigma_k}\right)\frac{\partial\langle\rho\rangle k}{\partial x_j}\right].$$

If compared to the conventional model for the TKE, the derived equation shows only one major difference that lies in the diffusion term. The diffusion term that emerges from the semi-local scaling methodology is a function of $\langle\rho\rangle k$ (instead of k), while the diffusion coefficient and the overall diffusion term are divided by $\sqrt{\langle\rho\rangle}$.

In analogy to the modified TKE equation, we derived the modified transport equations for the turbulent dissipation ε, specific turbulent dissipation ω, and the eddy viscosity in the Spalart-Allmaras turbulence model ν_{SA}. An additional modification we implement, specifically for the MK model, is to replace the non- dimensional wall distance y^+, and friction Reynolds number Re_τ, with their semi-local counterparts, namely the semi-locally scaled wall distance $y^\star$, and the semi-local friction Reynolds number $Re_\tau^\star$. For more details on the derivation the reader is refer to [2].

3.2 Turbulent Prandtl number

The turbulent Prandtl number relates the turbulent shear stress with turbulent heat flux, including the velocity and temperature gradient in the wall-normal direction as,

$$Pr_t = \frac{\langle\rho u_z" u_r"\rangle}{\langle\rho T" u_r"\rangle}\frac{\partial\langle T\rangle/\partial r}{\partial\langle u\rangle/\partial r}.$$

In the current study, we have used three approximations of the turbulent Prandtl number. These relations were developed for a flow with constant thermophysical properties.

- The Reynolds analogy is the simplest model for the turbulent heat flux, in which the turbulent Prandtl number is assumed constant. It assumes a strong analogy between momentum and scalar transport. The turbulent Prandtl number of 0.7 to 1.0 represents most gases in the log-layer [11].
- Kays in 1994 [11] proposed an approximation of the turbulent Prandtl number as a function of the ratio of turbulent and molecular viscosity. The algebraic expression — similar to a mixing length model for the eddy viscosity — is given as:

$$Pr_t = \frac{1}{C_1 + C_2\mu_\gamma - C_3\mu_\gamma^2\left[1 - exp\left(-C_4/\mu_\gamma\right)\right]},$$

DOI: 10.17185/duepublico/48872

where $\mu_\gamma = \mu_t/\langle\mu\rangle$ and the constants are $C_1 = 0.5882$, $C_2 = 0.228$, $C_3 = 0.0441$ and $C_4 = 5.165$.

- Irrenfried and Steiner [12] suggested an improvement of the turbulent Prandtl number by introducing an additional model parameter $\left(\gamma_{is} = \frac{1}{[\mathrm{Pr}_{t,\infty}+0.1\mathrm{Pr}^{0.83}]}\right)$ that depends on the molecular Prandtl number. This correlation for turbulent Prandtl number reads

$$1/\mathrm{Pr}_t = \frac{\gamma_{is} + C\,Pe_t\sqrt{2\left(\frac{1}{\mathrm{Pr}_{t,\infty}} - \mathrm{Pr}_{t,\infty}\right)}}{-(C\,Pe_t)^2\left[1 - exp\left(-\frac{1}{C\,Pe_t}\sqrt{2\left(\frac{1}{\mathrm{Pr}_{t,\infty}} - \gamma_{is}\right)}\right)\right]},$$

where $\mathrm{C} = 3.0$, and $\mathrm{Pe}_t = (\mu_t/\langle\mu\rangle)\mathrm{Pr}$ is the turbulent Peclet number. In the present study, we set $\mathrm{Pr}_{t,\infty} = 1.0$.

3.3 Buoyancy production term

The buoyancy production term in the transport equation of the turbulent kinetic energy is defined as,

$$G_k = -\langle u_z^{"}\rangle\left(\frac{\partial\langle p\rangle}{\partial z} - \frac{\partial\{\tau_{rz}\}}{\partial r}\right) \approx -\frac{\langle\rho\rangle}{Fr_0^2}\langle u_z^{"}\rangle.$$

The buoyancy production can be further simplified, using the Favre decomposition and relating the density fluctuation with the temperature fluctuations ($\langle\rho' u_z'\rangle = \beta_T\langle\rho u_z' T'\rangle$), as

$$G_k = -\frac{1}{Fr_0^2}\beta_T\langle\rho u_z' T'\rangle,$$

where the thermal expansion coefficient is defined as $\beta_T = -1/\langle\rho\rangle(\partial\rho/\partial T)$. The closure of the $\langle\rho u_z' T'\rangle$ term is generally accomplished with simple gradient diffusion hypothesis. However in the present study, we have approximated the buoyancy production with the Generalized Gradient Diffusion Hypothesis (GGDH), because it includes the anisotropic turbulent diffusivity using the Reynolds shear stress [13]. Using the GGDH, the buoyancy production is modelled as

$$\langle\rho u_z' T'\rangle = -C_t T_\tau\left(\langle\rho u_z^{"} u_r^{"}\rangle\frac{\partial T}{\partial r} + \langle\rho u_z^{"} u_z^{"}\rangle\frac{\partial T}{\partial z}\right),$$

where C_t is a positive constant equal to 0.333. This model requires the turbulent time scale T_τ, which for a $k-\varepsilon$ and a $k-\omega$ model is given by $T_\tau = k/\varepsilon$ and $T_\tau = 1/\omega$, respectively. For the Spallart-Allmaras model [16], buoyancy production is not taken into account.

4. CFD CALCULATIONS

4.1 Numerical setup

An in-house RANS code solves the governing equations — with a Poisson solver for the pressure correction — for momentum in radial and axial direction, enthalpy and turbulent scalars; the latter is dependent on the turbulence model. These equations are solved using a stagger space grid. A second-order central difference scheme and a Euler time integration scheme are used for the discretization in space and time, respectively. We used a maximum time step of 10^{-3} seconds. The diffusion terms in r-direction are treated implicitly, while the other terms are discretized explicitly.

The simulation setup consists of two parts as depicted in figure 3. First, an inflow generator is used to achieve a fully developed turbulent pipe flow. Periodic inlet and outlet boundaries and an isothermal flow are enforced to generate the inflow for the developing simulation. Afterwards, the fully developed profile is fed as the inlet boundary condition for the simulation of the developing pipe flow, which is uniformly heated from the wall.

The numerical domain of the pipe is axis-symmetric with a uniform discretization in the stream- wise direction ($N_z = 768$) and a non-uniform discretization in the wall-normal direction ($N_r = 192$). A hyperbolic tangent function is used to cluster the mesh points near the wall in order to ensure $y^+ < 1$ in the first mesh cell; no wall function is used. A grid convergence analysis was carried out for all the simulated cases to ensure mesh-independent results.

4.2 Results

This section of the paper reports the outcome of the RANS simulations of the upwards flowing CO_2 in the heated vertical pipe test cases. As mentioned in section 3, the compressible NS equations are coupled to three turbulence models —the MK, the SST, and the SA turbulence models. We assess the impact of including density corrections in these turbulence models on predicting the heat transfer. We refer to the turbulence models with the density modifications as MK-ρ, SST-ρ and SA-ρ.

4.2.1 Test case 1, Bae et al. [17]

The experiments from Bae et al. [17] are solved using the selected turbulence models with and without density modifications and the turbulent Prandtl number is approximated as $\mathrm{Pr_t} = 0.9$.

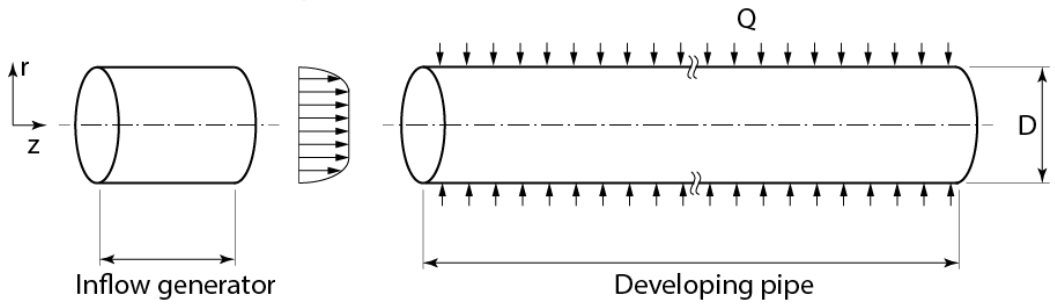

Figure 3. Numerical set-up for the CFD simulations

DOI: 10.17185/duepublico/48872

Most of the turbulence models accurately estimate the wall temperature for case 1 with a heat flux of 29.3 kW/m^2, see figure 4a. One exception is the SST-ρ model, but as already mentioned in our previous study, Otero et al. [2], the density modifications have detrimental effects on this specific model. The standard MK model is another model that lacks accuracy when compared to the experiments. With the density modifications, the MK-ρ model improves considerably, resulting in a close match with the experimental data. The SA and SA-ρ both have a similar prediction; these models slightly overestimate the wall temperature below the pseudo-critical enthalpy. The SST model accurately matches the experimental values. For this particular experiment, the CFD simulations have sufficient accuracy with the exception of the MK and SST-ρ models. Therefore, we will not include these two models in the remainder of this article

For the experiment with a higher heat flux (q" = 48.8 kW/m^2), the results with all the turbulence models agree qualitatively with the experiments; the SST-ρ and MK models are not included. Moreover, none of the models are able to reproduce the wall temperature distribution quantitatively (see figure 4b). The SST model does not estimate any heat transfer deterioration, with the wall temperature below the measured values. The MK-ρ model overestimates the wall temperature until a bulk enthalpy of ≈ −40 kJ/kg, where a strong heat transfer deterioration is predicted. The SA models with and without density modifications qualitative predict the heat transfer deterioration but underestimating the wall temperature. Above the bulk enthalpy of −200 kJ/kg, all models are close to the experimental data, except the MK-ρ model.

4.2.2 Test case 2, Kim et al. [18]

For test case 2, we will focus only on the experiments from Kim et al. [18] with heat transfer deterioration; these experiments have a heat flux of 23 kW/m^2 and 30 kW/m^2, see table 1. For these results, we approximate $Pr_t = 0.9$.

SA and SA-ρ are the only turbulence model able to reproduce heat transfer deterioration for the case 2 with a heat flux of 23 kW/m^2, see figure 5a. The two peaks in wall temperature are represented qualitatively, but not at the exact location. The rest of models cannot predict heat transfer deterioration. For case 2, 23 kW/m^2 is the value of heat flux where heat transfer deterioration starts to occur, for example for 20 kW/m^2 no deterioration is observed in the experiments.

All the turbulence models can reproduce heat transfer deterioration for a heat flux of 30 kW/m^2 (see figure 5b). Consistent with the previous experiment, the SA models are capable of predicting the sudden increase in wall temperature but again at a wrong location. The largest wall temperature peak of the SST and MK-ρ models occurs upstream from the measured data. Moreover, the SA, SA-ρ, and MK-ρ overestimate the wall temperature at the peak, the SST model underestimates it. The wall temperature trends after this point differ among the models. The SA and SST models tend to a lower wall temperature as if the heat transfer deterioration has been completed. Although overestimating the wall temperature, the MK-ρ model predicts qualitatively the wall temperature tendency with a steady increase in wall temperature at the outlet section of the pipe (z/D > 80).

The CFD simulation results from this second case for all four models are comparable to the inlet section of the high flux experiment of Bae et al. [17] (figure 4b). First, the SST model barely predicts heat transfer deterioration. Second, the SA and SA-ρ models predict the heat transfer deterioration earlier than observed in the experiments. Finally, the MK-ρ model follows the trend of the experiments qualitatively during the heat transfer deterioration. However, the performance of the turbulence model is not satisfactory. Therefore, we test different approximation of the turbulent Prandtl number with the expectation of a better approximation of the turbulent heat flux.

4.2.3 Turbulent heat transfer modelling:

In this section, we investigate different methods to model the turbulent heat transfer, more specifically the turbulent Prandtl number. We consider only Kim et al [18] experiments. We present the results for two RANS models: MK-ρ with an approximation of the turbulent Prandtl number: the Reynolds analogy (Pr_t=0.9) and two algebraic equations [11, 12], and SST with different constant values of the turbulent Prandtl number. The goal of this investigation is to evaluate the influence of the turbulent Prandtl model on the overall performance of the CFD simulation.

Both algebraic equations improve the prediction of the peaks for the wall temperature in the MK-ρ model, see figure 6a. Irrenfried's correlation predicts the second temperature peak. On the other hand, Kay's correlation estimates the first temperature peak accurately but predicts the second peak too early. Compared to the constant Prandtl number, the performance of the MK-ρ model is enhanced when coupled to algebraic equations for Pr_t. Still, compared to experimental data, the prediction of the turbulence model is not accurate.

The turbulent heat flux is inversely proportional to Pr_t; the lower the Pr_t value is, the higher the turbulent heat flux. Figure 6b shows the results obtained with the SST model with four different constant values of turbulent Prandtl number: 0.4, 0.9, 1.0, and 1.4. The model with the lowest turbulent Prandtl number shows no trace of heat transfer deterioration. The buoyancy effect and heat transfer deterioration increase for higher turbulent Prandtl numbers. The value that better matches the measured data is $Pr_t = 1$, rather than the commonly used value of 0.9. These two constant Pr_t values give different wall temperature behavior, especially around the temperature peak. As expected, the turbulent Prandtl number considerably influences the prediction of the heat transfer deterioration. However, there is hardly any qualitative difference downstream for z/D > 100.

DOI: 10.17185/duepublico/48872

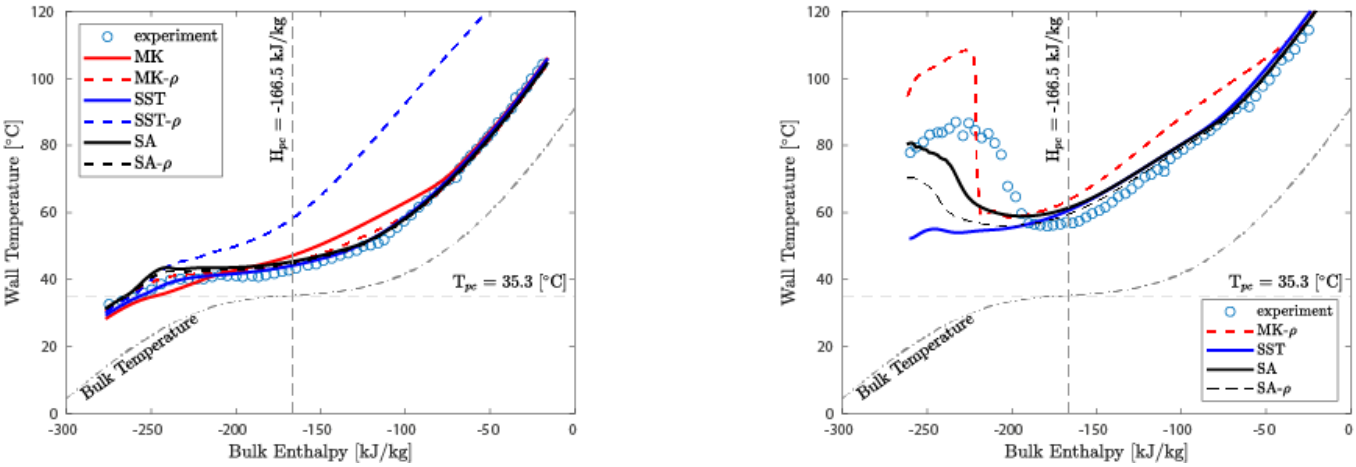

Figure 4. Wall temperature distribution as a function of the pipe stream-wise distance calculated with different RANS models (a) q" =29.3 kW/m^2 and (b) q"= 48.8 kW/m^2 compared to experiments [17]

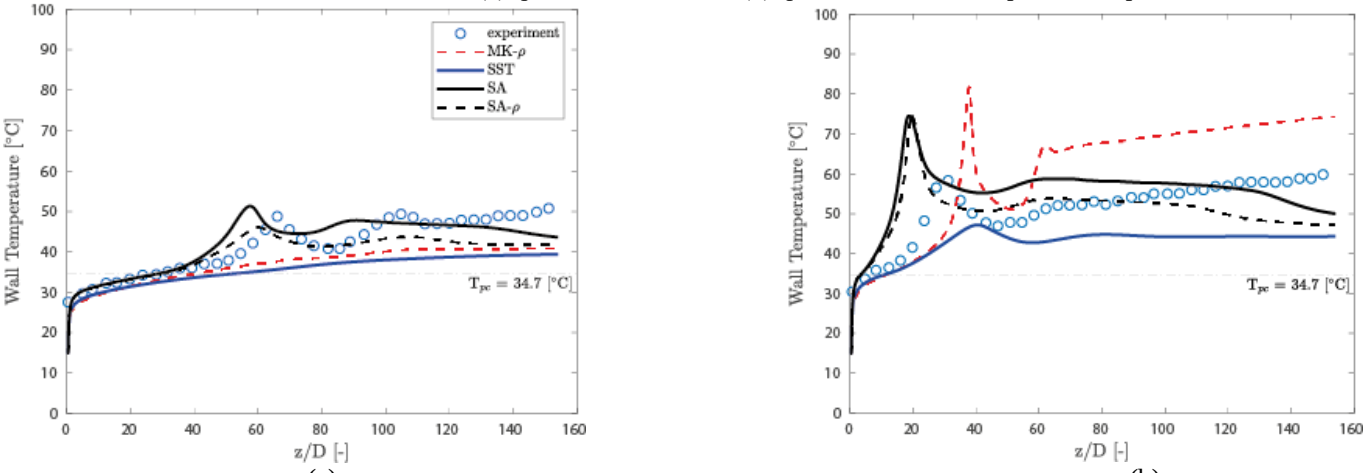

Figure 5. Wall temperature distribution as a function of the pipe stream-wise distance calculated with different RANS models (a) q" =23 kW/m^2 and (b) q"= 30 kW/m^2 compared to experiments [18]

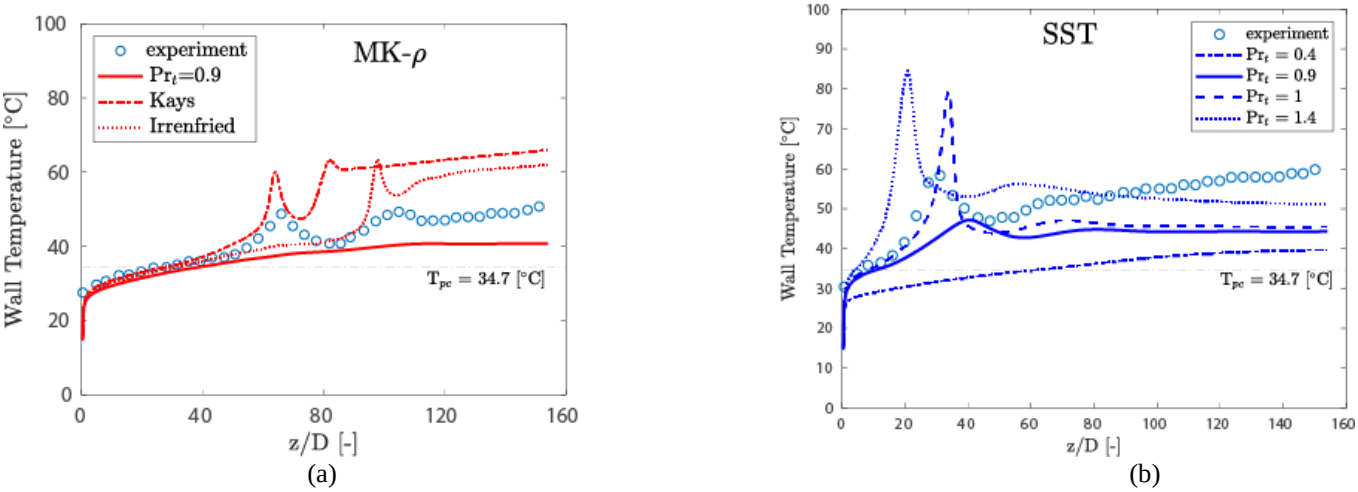

Figure 6. Wall temperature distribution as a function of the pipe stream-wise distance (a) q" =23 kW/m^2 calculated with MK-ρ and (b) q"= 30 kW/m^2 calculated with SST compared to experiments [17, 18]

DOI: 10.17185/duepublico/48872

The turbulent Prandtl number approach is quantitatively unsuccessful when buoyancy effects cannot be neglected. Due to the influence of buoyancy and the development of heat deterioration, an inflection point develops in the streamwise velocity profile, but not in the temperature field [10, 22]. In such a case, Pr_t will tend to infinity (see definition in section 3.2). Therefore, for a better approximation of the heat transfer in a supercritical flow with heat transfer deterioration, the turbulent heat flux should be modelled with an alternative method, for example with the turbulent thermal diffusivity [13, 23].

5. CONCLUSION

This paper analyzes different models to predict the heat transfer of supercritical CO_2 flowing upwards in a pipe at conditions with and without heat transfer deterioration. The results are compared with experiments from literature.

Three different turbulent models with and without density correction — as proposed in our previous study [2] — are analyzed. Most of these turbulence models accurately predict heat transfer in the absence of heat transfer deterioration; the standard Myong and Kasagi and the modified Menter's $\boldsymbol{k-\omega}$ SST models are the exceptions. However, heat transfer deterioration cannot be predicted by the investigated turbulence models. For this reason, we investigated the influence of the turbulent Prandtl number on the heat transfer for conditions when heat transfer deterioration occurs. Two different algebraic models for the turbulent Prandtl number are coupled with the turbulence models. The results obtained showed that the algebraic Prandtl number models — derived for constant property flows — gave encouraging results; they are able to quantify heat deterioration. However, the calculated wall temperature is quantitatively inaccurate. Future works will include models of the turbulent thermal diffusivity for the turbulent heat flux to predict the heat transfer of supercritical CO_2 flowing upwards in a pipe at conditions with heat transfer deterioration

NOMENCLATURE

ACRONYMS

DNS	Directed numerical simulation
EOS	Equation of State
MK	Myong-Kasagi (eddy viscosity model)
RANS	Reynolds-Averaged Navier-Stokes
SA	Spalart-Allmaras (eddy viscosity model)
SEV	Standard eddy viscosity model
SLS	Semi-local scaling
SST	Shear stress transport (eddy viscosity model)
TKE	Turbulent kinetic energy

SYMBOLS

c_p	specific heat at constant pressure
D	pipe diameter
Fr	Froude number
g	gravity
G	mass flux
G_k	Buoyancy production of turbulent kinetic energy
H	specific enthalpy
k	turbulent kinetic energy
N	number of discretization cells
p	pressure
Pe_t	turbulent Peclet number
P_k	Production of turbulent kinetic energy
Pr	Prandtl number
Pr_t	turbulent Prandtl number
q"	heat flux
r	wall-normal length
Re_τ	friction Reynolds number (locally scaled)
$Re_\tau^\star$	friction Reynolds number (semi-locally scaled)
S_{ij}	mean rate of strain tensor
T	temperature
T_τ	turbulent time scale
u	velocity
u_τ	friction velocity (locally scaled)
$u_\tau^\star$	friction velocity (semi-locally scaled)
y^+	Scaled wall distance (locally scaled)
$y^\star$	Scaled wall all distance (semi-locally scaled)
z	stream-wise length

GREEK

β_T	thermal expansion coefficient
δ_{ij}	Kronecker delta (δ_{ij}=0 if $i \neq j$ and δ_{ij}=1 if $i = j$)
λ	thermal conductivity
ε	dissipation rate of k
ρ	density
τ	shear stress
μ	viscosity
μ_τ	eddy viscosity
σ_k	constant of the eddy viscosity model
ω	specific dissipation rate of k

SUBSCRIPTS

0	inflow
cr	critical
r	wall-normal direction
t	turbulent
w	wall
z	stream-wise direction

SUPERSCRIPTS/ACCENTS/OPERATORS

ϕ^*	dimensional quantity
ϕ	locally scaled quantity
$\hat{\phi}$	semi-locally scaled quantity
$\langle\phi\rangle$	Reynolds averaging
ϕ'	Reynolds fluctuation
$\{\phi\}$	Favre averaging
ϕ"	Favre fluctuation

ACKNOWLEDGEMENTS

The authors thank the Netherlands Organization for Scientific Research (NWO) who partially funded this research through the grant with project number 14711.

DOI: 10.17185/duepublico/48872

REFERENCES

[1] He, W.S. Kim, J.H. Bae, Assessment of performance of turbulence models in predicting supercritical pressure heat transfer in a vertical tube, In International Journal of Heat and Mass Transfer, Volume 51, Issues 19–20, 2008, Pages 4659-4675.

[2] G. J. Otero Rodriguez, A. Patel, R. Diez Sanhueza, and R. Pecnik, Turbulence modelling for flows with strong variations in thermo-physical properties. In International Journal of Heat and Fluid Flow, 73, 2018.

[3] J. Dyreby, Modeling the supercritical Carbon Dioxide Brayton Cycle with Recompression, PhD Thesis, University of Wisconsin, Madison (2014).

[4] L.F. González-Portillo, J. Muñoz-Antón, J.M. Martínez-Val, Thermodynamic mapping of power cycles working around the critical point, Energy Convers. Manag. 192 (2019) pp. 359-373.

[5] Neises, T. and Turchi, C. A comparison of supercritical carbon dioxide power cycle configuration with an emphasis on CSP applications, Energy Procedio (2014), 49 1187-1196.

[6] I. Pioro, S. Mokry, Heat Transfer to fluids at supercritical pressure, in A. Belmiloudi (Ed.), Theoretical Analysis, Experimental Investigations and industrial systems, IntechOpen, 2011, pp. 481-504.

[7] Fages, Jacques, et al. "Particle generation for pharmaceutical applications using supercritical fluid technology." *Powder Technology* 141.3 (2004): 219-226.

[8] J. D. Jackson, Supercritical heat transfer, in: A-to-Z Guide to Thermo-dynamics, Heat and Mass transfer, and Fluids engineering, Vol, V, Begellhouse, 1997.

[9] J. H. Bae, J. Y. Yoo, and H. Choi. Direct numerical simulation of turbulent supercritical with heat transfer, Journal of Physics of Fluids, (April), 2005.

[10] H. Nemati, A. Patel, B.J. Boersma, R. Pecnik, Mean statistics of a heated turbulent pipe flow at supercritical pressure, International Journal of Heat and Mass transfer, 83 (2015) 741-752.

[11] W. M. Kays, Turbulent Prandtl number where are we? Journal of Heat Transfer 116 (2) (1994) 284-295.

[12] C. Irrenfried, H. Steiner, DNS based analytical p-function model for RANS with heat transfer at high Prandtl numbers. International Journal of Heat and Fluid flow, 66 (2017) 217-255.

[13] G. Zhang, H. Zhang, H. Gu, Y. Yang, X. Cheng, Experimental and numerical investigation of turbulent convective heat transfer deterioration of supercritical water in vertical tube, Nuclear Engineering and Design 248 (2012) 226-237.

[14] N. Myong, H.K. and Kasagi. A new Approach to the Improvement of k-e turbulence model for wall-bounded shear flows. JSME, 33(2), 1990.

[15] F. R. Menter. Zonal Two Equation k-w, Turbulence Models for Aerodynamic Flows. AIAA paper, page 2906, 1993. doi: 10.2514/6.1993-2906.

[16] A. Spalart, S, Allmaras. A One-Equatlon Turbulence model. doi: 10.2514/6.1992-439.

[17] Y.Y. Bae, H. Y. Kim, D. J. Kang, Forced and mixed convection heat transfer to supercritical CO_2 vertically flowing in a uniformly heated circular tubes. In Experimental Thermal and Fluid Science, 34 (8), 2010, pages 1295-1308.

[18] J.K. Kim, H.K. Jeon, J. Y. Yoo, J.S. Lee, Experimental study on heat transfer characteristics of turbulent supercritical flow in vertical circular/ non-circular tubes, in the 11th International Topical Meeting on Nuclear Reactor Thermal-Hydraulics, 2005.

[19] O. Kunz and W. Wagner. The gerg-2008 wide-range equation of state for natural gases and other mixtures: an expansion of gerg-2004. Journal of chemical & engineering data, 57(11): 3032-3091, 2012.

[20] P. Huang, P. G., Coleman, G. N., Bradshaw. Compressible Turbulent channel flows, DNS results and modeling. JFM, (1995): 185-218, 1995.

[21] A. Pecnik, R., Patel. Scaling and Modelling of turbulence in variable property channel, Journal of fluid Mechanics 2017.

[22] H. Nemati. Direct Numerical Simulation of turbulent heat transfer to fluids at supercritical pressures (Doctoral dissertation), Retrieved from the library's database of the Delft University of Technology, 2016.

[23] Kenjereš, S., S. B. Gunarjo, and K. Hanjalić. "Contribution to elliptic relaxation modelling of turbulent natural and mixed convection." *International Journal of Heat and Fluid Flow* 26.4 (2005): 569-586.

DOI: 10.17185/duepublico/48872

DOI: 10.17185/duepublico/48872
URN: urn:nbn:de:hbz:464-20190927-115117-2